Reviewed Preprint
v1 • February 18, 2026
Not revised

Reviewed Preprint
v2 • April 22, 2026
Revised by authors

# Bifunctional Architecture Enables Substrate Catalysis and Channeling in *Paracoccus* TMAO Demethylase

**Trung Thach[a], KanagaVijayan Dhanabalan[a], Shiwangi Maurya[b], Yu Han-Hallet[c], Senwei Quan[d], Jane Allison[d], Gurunath Ramanathan[b], Ramaswamy Subramanian[a,e]**

[a]Department of Biological Sciences, Purdue University, West Lafayette, United States • [b]Department of Chemistry, Indian Institute of Technology Kanpur, Kanpur, India • [c]Bindley Bioscience Center, Purdue University, West Lafayette, United States • [d]School of Biological Sciences, University of Auckland, Auckland, New Zealand • [e]Weldon School of Biomedical Engineering, Purdue University, West Lafayette, United States

**For correspondence:** ttthach@purdue.edu

**Competing interests:** No competing interests declared

**Reviewing editor:** Julien Roche, Iowa State University, United States



## eLife Assessment

This manuscript reports high-resolution cryo-EM structures of a trimethylamine N-oxide demethylase and advances the hypothesis that the enzyme is bifunctional, coupling TMAO demethylation to formaldehyde capture via an enclosed intramolecular tunnel. The structural findings remain **valuable**, particularly the unusual oligomeric architecture and proposed conduit for a reactive intermediate. While the revision improves clarity and addresses several technical concerns, the central mechanistic framework remains **incomplete**, with persistent concerns regarding the proposed catalytic mechanism and metal dependence.

https://doi.org/10.7554/eLife.109964.2.sa3

## Abstract

Substrate channeling enhances efficiency and prevents toxicity by directing unstable intermediates between active sites. Trimethylamine N-oxide demethylase (TDM) degrades trimethylamine N-oxide (TMAO) to dimethylamine and formaldehyde (HCHO), but the fate of HCHO has remained unclear. We report cryo-EM structures of TDM in apo, substrate-, and product-bound states that reveal a previously unknown channeling pathway. Combined structural, biochemical, and target molecular dynamics analyses show that HCHO is generated in a catalytic core and guided through a tunnel to a remote tetrahydrofolate (THF)-binding site, where it forms methylene-THF. Thus, TDM emerges as a bifunctional enzyme that unites TMAO demethylation with one-carbon transfer, providing a mechanistic explanation for its role in metabolic efficiency and detoxification.

## Introduction

Substrate channeling occurs in enzymatic reactions, where intermediates are transferred directly from one enzyme's active site to another, bypassing their release into the cellular environment. [1,2] This mechanism improves catalytic efficiency by minimizing intermediate loss, while simultaneously protecting cells from the damaging effects of unstable or toxic species. [1,2,3] Classic examples include glycolytic and amino acid metabolic enzymes, where covalent or noncovalent tunnels ensure safe and rapid passage of intermediates. [1,2,3] Despite its importance, structural evidence for substrate channeling remains limited, particularly in enzymes that couple detoxification with energy metabolism.

Trimethylamine (TMA) and its oxidized derivative trimethylamine N-oxide (TMAO) are abundant small molecules present in both marine organisms and the human gut microbiome.[4,5] TMA arises from microbial metabolism of dietary choline, carnitine, and other animal-derived nutrients, and is subsequently oxidized to TMAO by host flavin-containing monooxygenases.[4],[5] These metabolites are physiologically and clinically significant; elevated TMAO levels have been associated with cardiovascular disease and gastrointestinal cancer.[4,5] Conversely, in marine bacteria and certain gut microbes, TMAO serves as both an energy source and a carbon donor, fueling specialized catabolic pathways that convert it into downstream metabolites. [4,5,6]

A key enzyme in this process is trimethylamine N-oxide demethylase (TDM), which catalyzes the cleavage of a methyl group from TMAO to generate dimethylamine (DMA) and formaldehyde (HCHO).[6,7] Early biochemical studies revealed that TDM is a two-domain protein: an N-terminal domain that mediates TMAO demethylation, and a C-terminal domain structurally related to tetrahydrofolate (THF)-dependent enzymes, including the glycine cleavage T protein and dimethylsulfoniopropionate demethylase.[7,8,9] This homology led to the hypothesis that the C-terminal domain could utilize the HCHO intermediate to form methylenetetrahydrofolate (MTHF), thereby coupling detoxification with one-carbon transfer metabolism.[7,9] However, the molecular details of this bifunctional activity, how reactive formaldehyde is channeled and presented to the THF-binding site, have remained unresolved.

Here, we report cryo-EM structures of *Paracoccus* TDM captured in apo, substrate-bound, and product-bound states, providing the first high-resolution view of its dual-domain architecture (local resolution of 2.0 Å). Structural analysis revealed that the TMAO- and THF-binding pockets are separated by approximately 60 Å, raising the question of how formaldehyde is safely transferred. Tunnel mapping combined with target molecular dynamics simulations identified a continuous, negatively charged channel linking the two active sites, suggesting a structural basis for substrate channeling. Complementary biochemical assays and mass spectrometry confirmed that HCHO generated at the Core catalytic site is efficiently converted to MTHF at the C-terminal domain. Together, these results establish TDM as a bifunctional enzyme that unites TMAO demethylation with formaldehyde detoxification and one-carbon transfer, highlighting a microbial strategy to enhance metabolic efficiency while mitigating toxicity.

# Results and discussion

## Optimization of TDM Activity and Evidence for Bifunctionality

We first optimized purification and assay conditions for TDM by systematically varying salt concentration, pH buffer, and temperature. These analyses revealed a broad range, with the highest activity between pH 6.0 and 7.0 at 150 mM NaCl and 35-45 °C (Figure S1A–D). Under these conditions, TDM robustly demethylated TMAO, yielding HCHO with a $V_{max}$ of 156 nmol/min/mg and a $K_m$ of 1.33 mM (Figure 1A). Notably, these kinetic parameters indicate higher catalytic activity than the previously reported TDM from *Methylocella silvestris*, which exhibits a $K_m$ of 3.88 mM and a $V_{max}$ of 14.61 nmol/min/mg.[7] HPLC-MS confirmed the production of DMA as a co-product (Figure 1B), consistent with prior reports.[7] Notably, HCHO concentrations decreased upon addition of THF (Figure 1C), suggesting that HCHO may be further processed into MTHF (Figure 1D). Overall, these findings show that TDM carries out two linked reactions: TMAO demethylation at one active site, and the HCHO produced can condense with THF at the C-terminal domain, connecting TMAO breakdown to one-carbon metabolism.

## Cryo-EM Structures Reveal an Unusual Oligomeric Assembly

To elucidate the catalytic mechanism, we determined cryo-EM structures of apo TDM, a product-bound state (TMAO-soaked wild type), and a substrate-trapped mutant (D220A/D367A in complex with TMAO) (Figure 2A–B, S2, Table 1). TDM assembles into an unexpected 2 + 2½ oligomeric architecture (Figure 2A–C). Two full-length subunits form a highly symmetric core

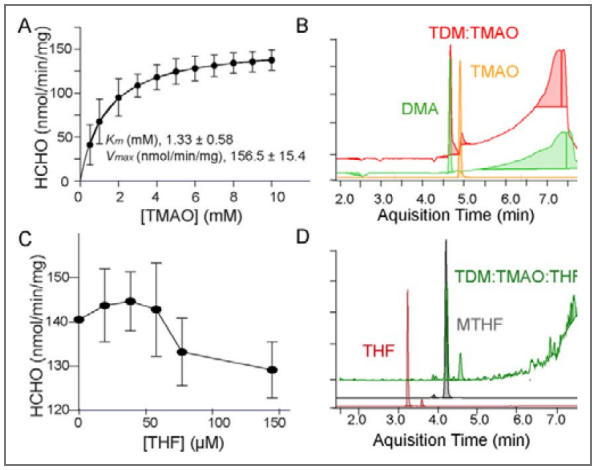


**Figure 1. TDM catalyzes two sequential reactions.**

(A) Steady-state kinetic analysis of TDM - producing HCHO, in response to varying concentrations of the substrate TMAO (n=3). (B) Representative HPLC-MS spectrum of DMA product from TDM:TMAO reaction. The standard curve for DMA is shown in green, and that for TMAO is shown in orange. The red trace shows the product of the reaction when TMAO is added to TDM, indicating the formation of DMA. Counts in the Y-axis. (C) Linear regression analysis demonstrates a concentration-dependent decrease in HCHO production when THF is included in the reaction mixture, suggesting THF-dependent consumption or conversion of HCHO. (D) Representative HPLC-MS confirming the formation of MTHF adduct as a product of the TDM:TMAO:THF reaction. The red, gray, and green lines represent the standard curves for THF, MTHF, and the reaction product when TMAO and THF were present with TDM, respectively.

dimer (RMSD = 0.12 Å over 787 Cα atoms), while two peripheral half-subunits consist solely of C-terminal THF-binding domains (Figure 2C). The core dimer interface is stabilized by extensive hydrogen-bonding and hydrophobic interactions (Figure S3).

Each catalytic core domain contains a conserved 3Cys:$Zn^{2+}$ motif (C285, C301, C365) essential for protein stability (Figure 2D, S4). Substitution of any of these cysteines with alanine led to aggregation, underscoring their structural importance. Elemental analysis (EDS and ICP–MS) confirmed zinc incorporation but excluded iron, yielding a Zn: protein ratio of ~1:2 (Figure S5A, B). This motif is analogous to $Zn^{2+}$ centers in cytidine deaminases,[10,11] alcohol dehydrogenases, and other Zn metalloenzymes.[12,13]

## $Zn^{2+}$-Dependent Organization at the Core Catalytic Domain

In TDM, $Zn^{2+}$ occupies a single, well-defined site within the core catalytic domain and plays a central non-redox role in substrate binding and organization of the active-site environment. Cryo-EM analysis of the TDM: TMAO complex reveals clear densities corresponding to the reaction products dimethylamine (DMA) and formaldehyde (HCHO) within the $Zn^{2+}$-containing active site (Figure 2E), supporting its direct involvement in substrate turnover. $Zn^{2+}$ coordinates the TMAO substrate via its oxygen atom and contributes to proper substrate positioning in concert with conserved residues D220, F327, and D367 (Figure 2E).

The cryo-EM structure of the TDM:DMA: HCHO complex shows both products retained within the active site, whereas in the D220A/D367A: TMAO mutant structure, the substrate remains trapped without substantial conformational changes relative to the wild-type enzyme (Figure 2E, F). Consistent with these observations, the F327A and D220A variants exhibit markedly reduced enzymatic activity, underscoring their importance in substrate recognition and active-site organization (Figure 2G). In contrast, mutation of D367, which participates in hydrogen bonding with the DMA product, results in a more modest (~10%) reduction in activity, consistent with a role in product stabilization rather than substrate binding or activation (Figure 2E–G).

Based on our structural and biochemical data, we propose a structurally informed working model for TMAO turnover by TDM (Scheme 1). In this model, $Zn^{2+}$ plays a non-redox role by polarizing the O–H bond of the bound hydroxyl, thereby lowering its $pK_a$. The D220 carboxylate functions as a general base, abstracting the proton to generate a hydroxide nucleophile. This hydroxide then attacks the electrophilic N-methyl carbon of TMAO, forming a tetrahedral carbinolamine (hemiaminal) intermediate. Subsequent heterolytic cleavage of the C–N bond leads to the release of HCHO. D220 then switches roles to act as a general acid, donating a proton to the departing nitrogen, thereby facilitating product release and regenerating the active site. This sequence allows a new water molecule to rebind $Zn^{2+}$, enabling subsequent catalytic turnovers. This proposed pathway is consistent with prior mechanistic studies, in which water addition to the azomethine carbon of a cationic Schiff base generates a carbinolamine intermediate, followed by a rate-limiting breakdown to yield an amino alcohol and a carbonyl compound, in the referenced case, an aldehyde.[14]

In particular, we observe no structural or biochemical support for an additional iron-binding site. Previous studies of TDM from *Methylocella silvestris* proposed an iron-dependent mechanism based on metal analysis and mutagenesis, in the absence of structural information. Distinct binding sites for $Zn^{2+}$ and non-heme $Fe^{2+}$ were not experimentally determined.[7,15] In contrast, our structural analyses consistently reveal a single metal-binding site occupied by $Zn^{2+}$. Even when TDM was expressed in LB medium supplemented with 0.5 mM $Fe(NH_4)_2SO_4$ (Figures S6A and S6B), we did not observe a second iron-binding site. Thus, $Zn^{2+}$ appears to function primarily as an organizational cofactor at the core catalytic domain, while the source of the oxidative chemistry required for demethylation remains unresolved.

| Structures<br>PDB<br>EMD | TDM-apo<br>9Q59<br>EMD-72223 | TDM:DMA:HCHO:THF<br>9Q5L<br>EMD-72239 | (DD):TMAO:THF<br>9Q5A<br>EMD-72224 |
|---|---|---|---|
| *Data collection and processing* | | | |
| Magnification | 105,000 | 105,000 | 105,000 |
| Voltage (kV) | 300 | 300 | 300 |
| Electron exposure ((e⁻/A□2) | 56.8 | 56.8 | 56.8 |
| Defocus range ((μm) | 0.8-2.0 | 0.8-2.0 | 0.8-2.0 |
| Raw pixel size ( A□) | 0.411 | 0.411 | 0.411 |
| Symmetry imposed | C2 | C2 | C2 |
| Number of initial particle images | 145,414 | 568,305 | 240,010 |
| Number of final particle images | 26,866 | 174,871 | 143,707 |
| Map resolution (A□) | 2.76 | 2.79 | 2.80 |
| FSC threshold | 0.143 | 0.143 | 0.143 |
| Map resolution range ( A□) | 2.5-5.0 | 2.5-5.0 | 3.0-5.0 |
| *Refinement* | | | |
| Initial model used | Alphafold model | Apo model | Apo model |
| Model resolution ( A□) | N/A | 2.8 | 2.8 |
| FSC threshold | 0.5 | 0.5 | 0.5 |
| Model resolution range ( A□) | N/A | 3.0-50 | 3.0-50 |
| Model composition | | | |
| Non-hydrogen atoms | 17878 | 17058 | 17917 |
| Protein residues | 2309 | 2196 | 2306 |
| Ligand: ZN | 2 | 2 | 2 |
| TMO | | | 2 |
| HCHO | | 2 | |
| DMN | | 2 | |
| B factors (A□2) | | | |
| Protein | 118.75 | 87.46 | 86.93 |
| Ligand | 144.67 | 89.10 | 90.75 |
| RMSD values | | | |
| Bond lengths ( A□) | 0.004 | 0.004 | 0.003 |
| Bond angles (°) | 0.586 | 0.608 | 0.501 |
| *Validation* | | | |
| Molprobity score | 2.22 | 2.32 | 2.02 |
| Clash score | 8.74 | 12.12 | 7.78 |
| Poor rotamer (%) | 2.98 | 2.63 | 2.18 |
| Ramachandran plot (%) | | | |
| Favored | 94.25 | 93.89 | 95.07 |
| Allowed | 5.49 | 6.01 | 4.80 |
| Outliers | 0.26 | 0.09 | 0.13 |

**Table 1.** **Cryo-EM data collection, refinement, validation and statistics**

**Figure 2. Overall architecture of TDM determined by cryo-electron microscopy.**

(A) Representative cryo-electron microscopy (EM) maps. (B) Overall structure of the complex, with each subunit colored differently. TDM adopts a 2 + $2^{1/2}$ complexation. The two half-domains of the complex are the C-terminal domains. (C) (C) Schematic illustration of TDM complexation. TDM monomers with N-terminal, Core, and C-terminal domains are colored forest, orange, and blue, respectively. The same coloring is used in panels A and B. (D) Close-up view of the 3Cys:$Zn^{2+}$ binding motif. (E) Close-up view of the interactions between DMA and HCHO products with the 3Cys:$Zn^{2+}$ motif. (F) The TMAO substrate is trapped in the 3Cys:$Zn^{2+}$ active site of the double D220A/D367A mutant. The density maps are shown and contoured at 3.0 σ with a carve of 2 Å. Bound small molecules are shown as ball-and-stick representations, amino acid residues as sticks, and hydrogen bonds as dashed lines. (G) Relative activity of TDM variants.

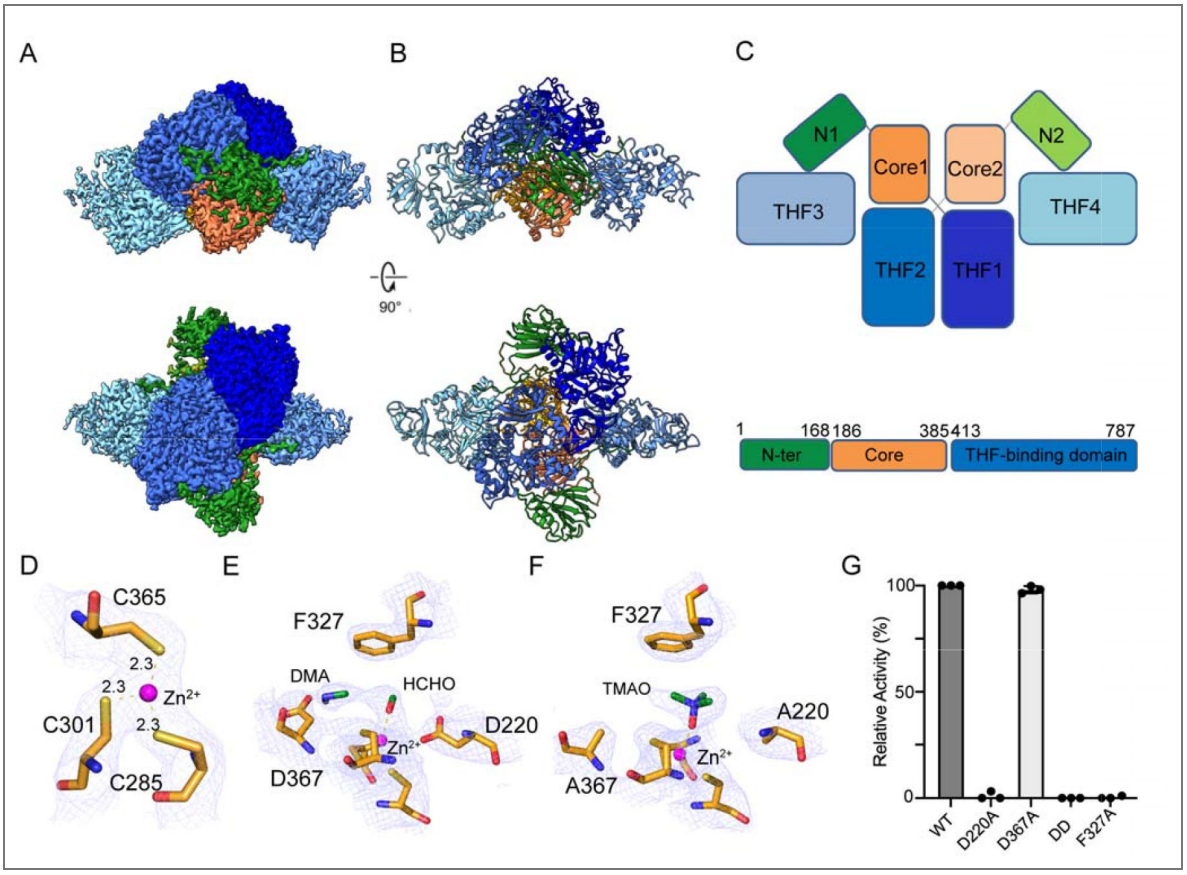


**Scheme 1. Structurally informed working model for TDM-mediated TMAO turnover.**

TMAO binds at a single $Zn^{2+}$-containing active site, where $Zn^{2+}$ plays a non-redox role in substrate coordination and organization of the catalytic environment. Conserved residues contribute to substrate positioning and product stabilization. D220 acts as the catalytic base.

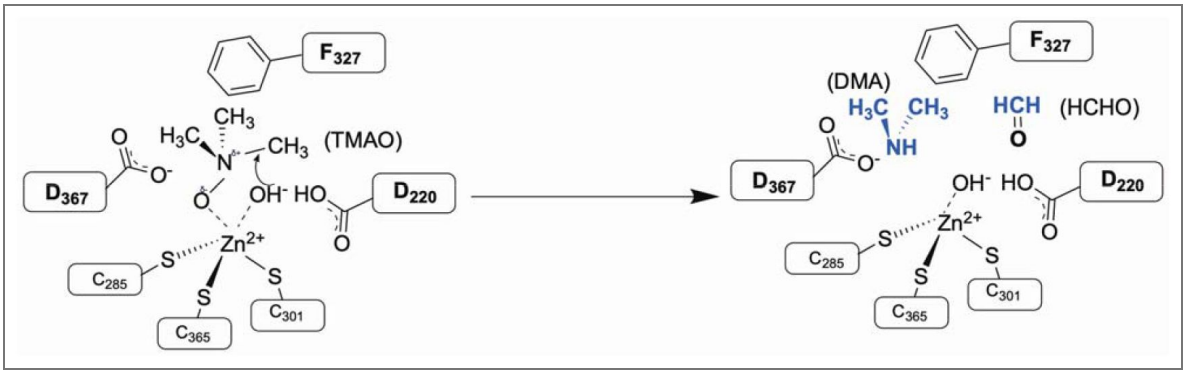

## Architecture and Binding Properties at THF-Binding Domain

The C-terminal THF-binding domain is positioned on the intramolecular face and forms extensive electrostatic interactions that are essential for stabilizing the central dimer interface (Figure S7A, B). Structural comparison revealed high similarity to a THF-binding protein, with superposition onto a T protein (PDB ID: 1WOO) yielding an RMSD of 1.18 Å over 371 Cα atoms (Figure S7C).

Cryo-EM density at the folate-binding site was consistent with that of THF binding, although resolution limitations and partial occupancy prevented complete ligand assignment (Figure 3A). Based on the structural homology, we modeled THF in the central cavity of the ring structure (Figure 3B). The pterin moiety of THF projected into the interior cavity, forming hydrophobic contacts with the aromatic folate-binding pocket (Figure 3B). Two positively charged residues, R480 and K782, located near the entrance of the binding funnel, likely engaged the polyglutamate tail via hydrogen bonding, complemented by π-stacking from F582 and F672 (Figure 3B). Similar binding modes have been observed in enzymes, such as T-proteins, aminotransferase domains, and dimethylglycine dehydrogenase.[17,18,19] ITC binding isotherms show a clear interaction between THF and TDM, with negligible heat change in the buffer control, confirming binding specificity. The dissociation constant (*Kd*) was determined to be approximately 149 nM (Figure 3C, S8).

## A Substrate Channel for Formaldehyde Transfer

High-resolution cavity mapping of the TDM:DMA:HCHO: THF complex revealed a continuous intramolecular tunnel that connects the $Zn^{2+}$-containing demethylase pocket to the distal THF-binding site (Figure 4A). This conduit begins at the formaldehyde release position within the catalytic pocket at the core domain (HA, HB) and terminates near the folate pterin ring at the C-terminal domain (TA, TB). The channel is predominantly lined with acidic residues and polar side chains, generating a strongly negative electrostatic potential (Figure 4A). Such electrostatics likely stabilize the partial negative oxygen of HCHO, guiding it through the tunnel while excluding bulk anions and minimizing leakage.

Geometrically, the tunnel exhibits a radius ranging between 2.6 and 5.0 Å, with the narrowest bottleneck of 2.6 Å positioned just before the folate-binding cavity (Figure 4B). This matches closely with the van der Waals dimensions of formaldehyde (~2.5 Å), suggesting evolutionary fine-tuning for selective transfer of this reactive one-carbon intermediate. Importantly, no alternative solvent-accessible exits were detected, indicating that HCHO is obligatorily channeled to the THF site rather than diffusing freely.

Coarse-grained target molecular dynamics simulations further supported this interpretation. Independent trajectories consistently identified two persistent tunnels, each connecting the $Zn^{2+}$ demethylation sites (HA, HB) to the corresponding folate-binding sites (TA, TB) in the two protomers (Figure 4C, S9). Within these trajectories, formaldehyde molecules entered the channel from the catalytic site, transiently interacted with acidic residues and ordered water molecules, and passed through narrow gating residues that rearranged to allow transit (Figure 4C). This dynamic yet persistent tunnel suggests a gated channeling mechanism that balances selectivity with throughput.

The channeling mechanism in TDM bears resemblance to classical substrate-channeling systems but with distinct architectural solutions. In tryptophan synthase, an ~25 Å hydrophobic tunnel delivers indole between two active sites,[20,21] whereas the glycine cleavage system employs a swinging lipoate arm on the H-protein to transfer intermediates between catalytic partners. [22,23] Dimethylglycine dehydrogenase also channels formaldehyde to THF, but does so through surface-proximal transfer rather than via a buried conduit,[9,19] while the PaaZ enzyme in phenylacetate catabolism uses electrostatic pivoting, in which a domain-swapped CoA arm swings the intermediate between domains, guided by conserved positive residues.[23] By contrast, TDM relies on a fully enclosed, negatively charged tunnel, a unique design optimized for formaldehyde, a small, highly diffusible, and cytotoxic intermediate.

**Figure 3.** **THF binding to TDM.**

(A) The THF-binding domain forms a cloverleaf of three subdomains (I-III), creating a central cavity that accommodates THF. EM density for THF is shown as a surface. (B) Close-up of the binding pocket highlighting hydrophobic and hydrogen-bonding residues that stabilize THF, colored according to their subdomain location in panel A. (C) ITC analysis confirms specific THF binding to TDM (blue), with negligible signal in buffer control (gray).

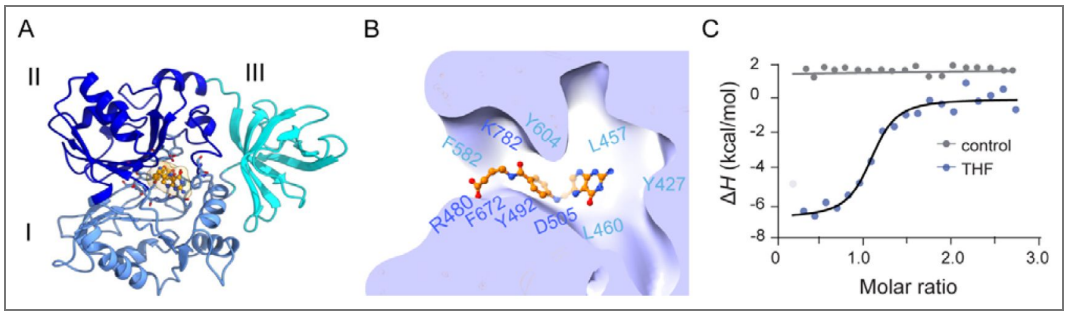


**Figure 4.** **HCHO channels from the active site to the THF-binding site in TDM complex.**

(A, B) Surface representations of the channels within the TDM complex colored according to either electrostatic potential or radius. (C) Tunnel analysis of a CG MD simulation suggests that HCHO in each chain can access the THF binding sites in chains A and B. The five top-ranked paths for chain A are shown in different colors. THF, DMA, and HCHO are depicted as spheres colored by the atom type. TA, TB, TC, and TD: THF molecules in chains A, B, C, and D, respectively; HA: chain A, HCHO.

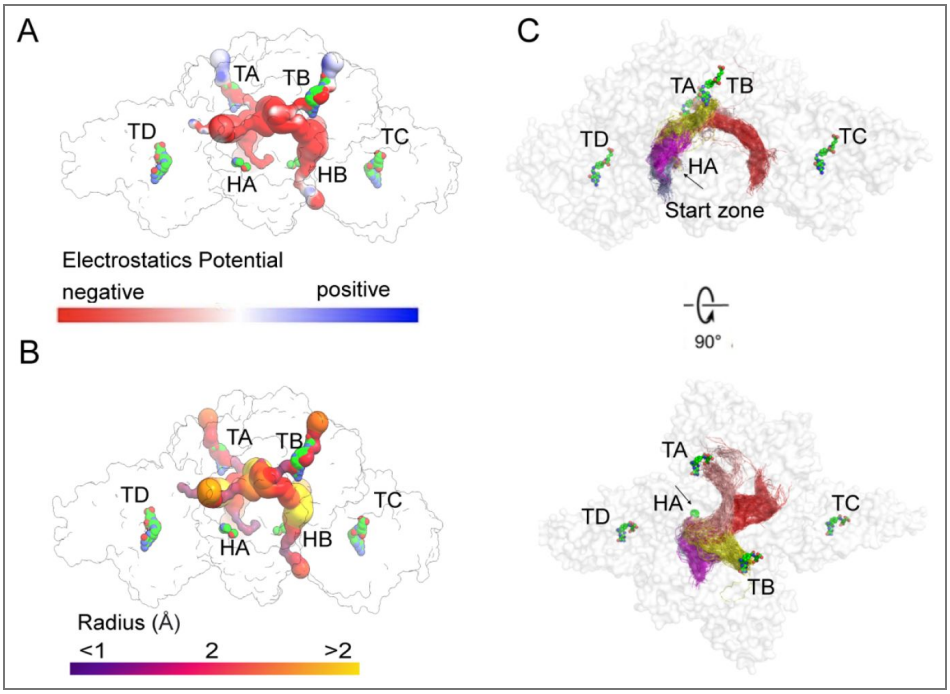

### Role of the N-terminal domain in TDM assembly and function

The function of the N-terminal domain in TDM has remained unclear, and sequence alignment across homologs reveals low evolutionary conservation in this region (Figure 5A). Cryo-EM analysis revealed two distinct interaction modes between the N-terminal and C-terminal domains, including an unexpected interdomain interface between the N-terminal region and a peripheral THF-binding domain (Figure 5B, S10, Video S1). This interface appears to tether the flexible N-terminus to the THF-binding domain, forming a structural bridge that may regulate the conformational transitions required for complex assembly and efficient substrate transfer. The interaction is stabilized by aromatic stacking between P14 and W476, charge interaction, along with extensive hydrophobic contacts that promote proper domain packing and interdomain communication (Figure 5B, S9).

Functional analyses further support this structural coupling. Deletion of the entire N-terminal region (Δ1–150) or the interfacial segment (Δ151–158) led to severe aggregation and loss of soluble protein, while removal of only the first 20 residues (Δ1–20) caused a modest (~10%) reduction in catalytic turnover (Figure 5C). These results indicate that the N-terminal domain not only stabilizes the quaternary architecture but may also facilitate allosteric coupling between the catalytic and folate-binding domains. Such dynamic coupling likely ensures efficient handoff of formaldehyde through the internal tunnel, synchronizing demethylation and one-carbon transfer reactions within the bifunctional TDM complex.

## Conclusion

Our results establish TDM as both a bifunctional enzyme and an integrated substrate-channeling system. By coupling TMAO demethylation with THF-dependent one-carbon transfer, TDM not only produces DMA and methylene-THF but also ensures immediate capture of formaldehyde, a highly reactive and cytotoxic intermediate. Structural, biochemical, and computational analyses reveal that this is achieved through a fully enclosed, negatively charged conduit that links the $Zn^{2+}$ catalytic core to the folate-binding site, thereby enhancing catalytic efficiency and preventing metabolite leakage.

Beyond defining the molecular basis of TDM activity, these findings highlight a general design principle: substrate channeling can evolve distinct architectures, hydrophobic tunnels, swinging arms, or electrostatic conduits, tailored to the physicochemical properties of the intermediate. The TDM structure expands this paradigm by revealing a tunnel optimized for formaldehyde transfer, underscoring microbial strategies for detoxification and metabolic efficiency. More broadly, this work provides a framework for re-engineering channeling systems in biocatalysis, synthetic biology, and microbiome modulation, where controlling the fate of reactive intermediates is central to both metabolic innovation and therapeutic applications.

## Experimental details

### TDM Construction, Expression, and Purification

The gene encoding full-length TDM (1-787) (WP_26356686) from *Paracoccus* sp. DMF was optimized for *E. coli* codons and cloned into the pET21a(+) plasmid with either a C-terminal 6xHis tag or an N-terminal strepII tag using NdeI and XhoI restriction enzymes. Site-directed mutagenesis involving substitutions or deletions was performed using specific PCR primers (Universal, USA). Plasmid isolation and purification from E. coli were performed using a DNA spin kit (Qiagen, Germany), and the identity of the DNA constructs was confirmed by sequencing (Genewiz, USA).

The TDM protein variants were expressed in *E. coli* BL21 (DE3) cells cultured in LB medium at 37 °C. Induction was achieved with 0.25 mM isopropyl β-D-1-thiogalactopyranoside (IPTG) at 18 °C for 16 h. Protein purification was performed by affinity chromatography using either Ni-NTA resin (Qiagen, Germany) or a strep-tag column (Cytiva, USA) in buffer A (20 mM Tris-HCl, pH 7.5, 250 mM NaCl, 1 mM TCEP, 300 mM imidazole, and 5% glycerol). Further purification steps included

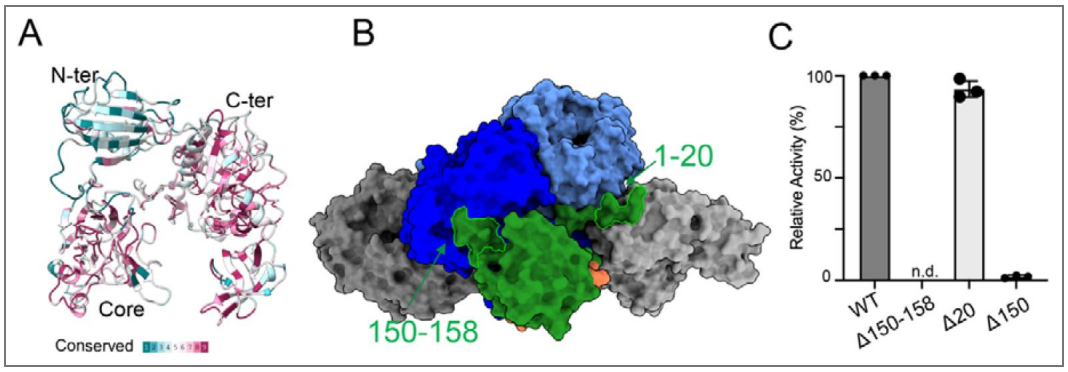


**Figure 5. The N-terminal domain is involved in the structural stability and assembly of proteins.**

(A) The evolutionary conservation of residue positions on the TDM structure is estimated based on phylogenetic connections among homologous sequences. (B) N-terminal domain was depicted as forest. Residues ranging from 1-20, 150-158 were highlighted. (C) Relative TDM activity of TDM mutants compared to that of WT variant.

passage through a 2 × 5 mL HiTrap Q column (GE Healthcare, USA) using buffer B (20 mM Tris-HCl pH 7.5, 200 mM NaCl, 1 mM TCEP, and 5% glycerol) for equilibration, and buffer C (20 mM Tris-HCl pH 7.5, 1000 mM NaCl, 1 mM TCEP, and 5% glycerol) for elution. Final purification was achieved using a Superdex 200 increase 10/300 GL column (Cytiva, USA) in buffer D (20 mM Tris-HCl, pH 7.5, 150 mM NaCl, and 5% glycerol). The purity of the relevant fractions was assessed by SDS-PAGE.

## TDM Activity Assay

Enzyme activity was assessed by measuring HCHO production from TMAO breakdown as described previously with minor modifications.[24] Briefly, enzymatic activity was evaluated in multiple buffering systems spanning a range of pH values. Maximal activity was observed in 10 mM MES buffer (pH 6.0) supplemented with 150 mM NaCl; this buffer was subsequently used for all kinetic analyses. Standard activity assays were performed in triplicate at room temperature. Each 50 µL reaction contained 2.5 µg of purified TDM in MES buffer and was initiated by the addition of TMAO to a final concentration of 10 mM. Reactions were incubated for 10 min, a time point confirmed to be within the linear range based on preliminary time-course experiments. For HCHO detection, 10 µL of the reaction mixture was combined with 25 µL of freshly prepared 0.2% (w/v) Purpald reagent dissolved in 1 M NaOH and 215 µL of Milli-Q water in a 96-well plate. After incubation for 20 min at room temperature, absorbance at 540 nm was measured using a SpectraMax G5 microplate reader. Formaldehyde concentrations were calculated from a standard curve generated using analytical-grade formaldehyde (0–180 µM). The Michaelis–Menten constant (Km) and maximum velocity (Vmax) were determined using the PRISM v.10.0.0 software. To evaluate HCHO reduction in the presence of THF, reactions were conducted with 5 mM TMAO and varying concentrations of THF ranging from 0 to 150 µM.

For the analysis of DMA, CH2-THF products, and other compounds, high-performance liquid chromatography (HPLC) coupled with Mass Spectrometry (MS) was employed. The analysis was performed using an Agilent 1290 Infinity II LC system coupled with an Agilent 6470 series QQQ mass spectrometer. Waters Acquity UPLC with a bridged ethylene hybrid hydrophobic interaction chromatography (2.1 mm × 150 mm, 1.7 µm) column was used for separation. The mobile phases were as follows: (A) 90% acetonitrile, 5% isopropanol, and 5% 200 mM ammonium formate (pH 3) and (B) 90% water, 5% acetonitrile, and 5% 200 mM ammonium formate (pH 3). The LC gradient was: 0 min, 0% B; 2 min, 0% B; 7 min, 98% B; 7.5 minutes, 98% B; 8 min, 0% B; 15 min, 0% B, with a flow rate of 0.3 mL/min.

Mass spectrometric analysis was performed using multiple reaction monitoring (MRM) in the positive electrospray ionization (ESI) mode. The ESI interface settings were as follows: gas temperature, 325°C; gas flow rate, 7 L/min; nebulizer pressure, 45 psi; sheath gas temperature, 250°C; sheath gas flow rate, 7 L/min; capillary voltage, 3800 V; nozzle voltage, 1000 V; and ΔEMV voltage, 300 V. The concentrations of TMAO, DMA, THF, and CH2-THF were determined using internal deuterated standards (TMAO-d9 and DMA-d6), and the data were analyzed using the Agilent MassHunter Quantitative Analysis (Version B.08.00).

## Cryo-EM data processing and structure determination

Image processing and structure determination involve several steps. Motion correction and image summation were conducted using MotionCor,[25] and defocus values were estimated using Gctf.[26] Particle picking was performed using the DoG Picker,[27] followed by initial reference-free 2D classification in CryoSPARC v.4.2.0.[28] Representative 2D class averages were selected, and particle refinement was performed through multiple rounds of 2D classification. Subsequently, an initial ab initio reconstruction was performed. The particles underwent 3D classification into five classes using a low-pass filtered initial reconstruction at 20 Å as a reference model. Multiple rounds of 3D classification were performed, and the optimal subset displaying clear structural features underwent heterogeneous refinement over six rounds, resulting in a high-quality, refined subset. These refined particles underwent homologous refinement, yielding a map with global resolution indicated by a Fourier shell correlation (FSC) of 0.143. The final volume map was computed with C2 symmetry using CryoSPARC, and local resolution was assessed using Phenix. The initial apo

model of the TDM was built in Coot v0.8.9,[29] referencing the alphafold structure.[30] Monomeric TDM structures were fitted into cryo-EM electron density maps using UCSF ChimeraX,[31] with subsequent iterative manual adjustments and rebuilding in Coot, including modeling of the N-terminal domain. Manual refinement was based on the electron density map quality in Coot, followed by real-space refinement in Phenix.[32] Validation included the analysis of FSC curves to assess model-map agreement and the evaluation of atomic model geometry using MolProbity.[33] Detailed refinement statistics are provided in Table 1. The pore-lining surfaces and receptor channels were analyzed using the MOLE software.[34] Visual representations were created using UCSF ChimeraX and PyMOL.[35]

## Molecular Dynamics simulations of enzyme tunnelling

Coarse-grained (CG) MD simulations of TDM were conducted using the GROMACS 2021.5 and Martini3 force fields with the Gō model.[36] The CG coordinates were generated from the TDM:DMA: HCHO structure via martinize2,[37] with the secondary structure assigned using DSSP.[38] The Gō contact map was created using the GōContactMap server with a Cα–Cα distance cutoff of 0.3– 1.1 nm and Gō potential of 9.414 kJ·mol$^{-1}$.[36]

The simulations employed periodic boundary conditions, with short-range interaction cutoff at 1.1 nm and long-range electrostatics handled by the reaction-field method.[39] The system was maintained at 316.16 K and a pressure of 1 bar. Initial energy minimization was performed until the forces were below 10 kJ·mol$^{-1}$·nm$^{-1}$, followed by solvation using INSANE[40] and addition of 0.15 M NaCl. The system contained 1324 $Na^+$/$Cl^-$ beads and 110,246 water beads in the simulation box.

The system was equilibrated for 5 ns with position restraints on the backbone beads, followed by 10 ns of unrestrained equilibration. The 10 μs production run used the velocity-rescale thermostat,[41,42] and Parrinello-Rahman barostat, with a 20 fs time step and coordinates saved every 500 ps for the production run. Tunnel calculations were performed using CAVER3.0.[43] The starting points for the tunnel calculations were defined by residues near HCHO (A282, T369, and S378). A 2.5 Å probe radius and time sparsity of 1 were applied to avoid redundant tunnel generation. The detected tunnels were clustered using a threshold of 5.0 and a frame reweighting coefficient of 1. Protein stability was evaluated by calculating RMSD, RMSF, and Rg using *gmx rms*, *gmx rmsf*, and *gmx gyrates*, respectively.

## Isothermal Calorimetry (ITC)

ITC measurements were performed using a NANO ITC system (TA Instruments) to evaluate the binding affinities of TDM and THF at 20 °C. The compound solution was equilibrated with protein buffer D, and all protein and compound solutions were prepared in the same degassed buffer before use. ITC cells were loaded with 250 μl of TDM protein (5 μM) and titrated with THF (80 μM). Titration involved injecting 1 μl of the substrate into the protein solution, followed by 19 injections of 2.45 μl each. The stirring rate was set at 200 rpm. For control experiments, the buffer was injected into the protein alone. Equilibrium association constants were calculated by fitting reference-corrected data using the binding model supplied by the manufacturer.

## Energy-dispersive X-ray spectroscopy analysis (EDAX)

Ten microliters of TDM protein at a concentration of 100 μM was dropped on the silicon wafer and vacuum dried. After drying, the samples were gold-coated (~ 10 nm) and analyzed using a CARL ZEISS EVO 50. Buffer was used as a control experiment.

## Inductively coupled plasma-mass spectrometry (ICP-MS)

ICP-MS experiments were conducted using trace metal-grade nitric acid (HNO3, 3% v/v), which was purified in-house by sub-boiling point distillation, as the sample matrix. ICP-MS analyses were performed using an Agilent Technologies 7500 ICP-MS instrument, while ICP-OES was conducted using a Perkin Elmer Optima 5300DV Optical Emission Spectrometer. Calibration standards were

freshly prepared by diluting the stock solutions (Sigma-Aldrich) in 3% HNO3 and doubly deionized water. Approximately 2.4 mg of protein was diluted in a 3% HNO3 matrix for metal analysis, and zinc concentrations were measured using the emission line at 213.857 nm.

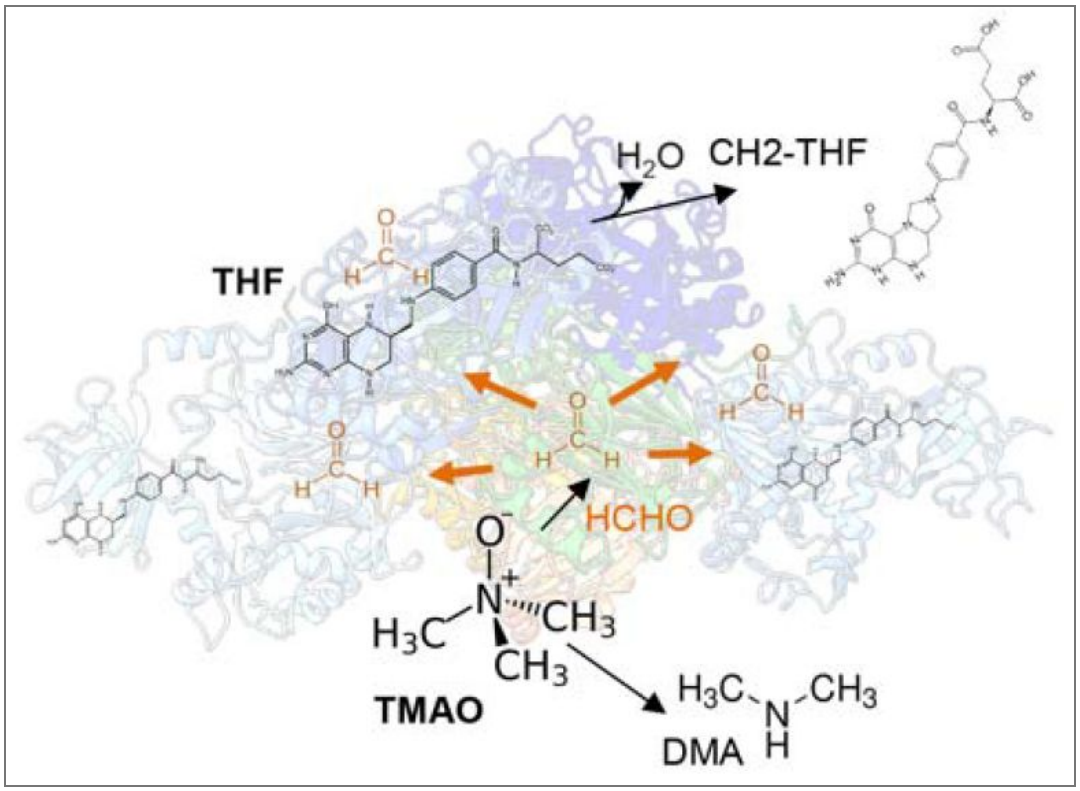

## Data availability

Cryo-EM data have been deposited in EMD and PDB. All data generated or analyzed during this study are included in the manuscript and supporting files; source data files have been provided for all figures.

## Acknowledgements

Special thanks go to Dr. Robert Stahelin for granting access to the ITC machine; Dr. Na Gou for ICP-MS analysis; Dr. T. Klose and Dr. F. Vago for cryo-EM, and S. Wilson for computation. We acknowledge the Purdue cryo-EM facility for access to instrumentation for data collection, and the New Zealand eScience Infrastructure for high-performance computing.

## Additional information

### Author Contributions

TT, KD, and SM conducted cellular and biochemical studies. YH conducted HPLC-MS. SQ and JR performed MD simulations. TT, GR, and RS were involved in designing the experiments and developing this project. TT and RS were involved in the structure determination, map interpretation, and result analysis. All authors participated in manuscript preparation and review.

### Author ORCID iDs

**Trung Thach**: https://orcid.org/0000-0001-8395-0623
**KanagaVijayan Dhanabalan**: https://orcid.org/0000-0001-8636-2616
**Ramaswamy Subramanian**: https://orcid.org/0000-0002-6709-190X

## Additional files

***supplementary***

***Video S1.***

## References

[1] **Leys D.,** Basran J., Scrutton N. S. (2003) Channelling and formation of 'active' formaldehyde in dimethylglycine oxidase. *The EMBO Journal* **22**:4038-4048 https://doi.org/10.1093/emboj/cdg395 | PubMed

[2] **Miles E. W.,** Rhee S., Davies D. R. (1999) The Molecular Basis of Substrate Channeling *. *Journal of Biological Chemistry* **274**:12193-12196 https://doi.org/10.1074/jbc.274.18.12193 | PubMed

[3] **Pareek V.,** Sha Z., He J., Wingreen N. S., Benkovic S. J. (2021) Metabolic channeling: predictions, deductions, and evidence. *Molecular Cell* **81**:3775-3785 https://doi.org/10.1016/j.molcel.2021.08.030 | PubMed

[4] **Querio G.,** Antoniotti S., Geddo F., Levi R., Gallo M. P. (2023) Modulation of Endothelial Function by TMAO, a Gut Microbiota-Derived Metabolite. *International Journal of Molecular Sciences* **24**:5806 https://doi.org/10.3390/ijms24065806 | PubMed

[5] **Ilyas A.,** Wijayasinghe Y. S., Khan I., El Samaloty N. M., Adnan M., Dar T. A., Poddar N. K., Singh L. R., Sharma H., Khan S. (2022) Implications of trimethylamine N-oxide (TMAO) and Betaine in Human Health: Beyond Being Osmoprotective Compounds. *Frontiers in Molecular Biosciences* **9** https://doi.org/10.3389/fmolb.2022.964624 | PubMed

[6] **Lidbury I.,** Murrell J. C., Chen Y. (2014) Trimethylamine N-oxide metabolism by abundant marine heterotrophic bacteria. *Proceedings of the National Academy of Sciences* **111**:2710-2715 https://doi.org/10.1073/pnas.1317834111 | PubMed

[7] **Zhu Y.,** Ksibe A. Z., Schäfer H., Blindauer C. A., Bugg T. D. H., Chen Y. (2016) O2-independent demethylation of trimethylamine N-oxide by Tdm of Methylocella silvestris. *The FEBS Journal* **283**:3979-3993 https://doi.org/10.1111/febs.13902 | PubMed

[8] **Wang X.-J.,** Zhang N., Teng Z.-J., Wang P., Zhang W.-P., Chen X.-L., Zhang Y.-Z., Chen Y., Fu H.-H., Li C.-Y. (2021) Structural and Mechanistic Insights Into Dimethylsulfoxide Formation Through Dimethylsulfide Oxidation. *Frontiers in Microbiology* **12** https://doi.org/10.3389/fmicb.2021.735793 | PubMed

[9] **Augustin P.,** Hromic A., Pavkov-Keller T., Gruber K., Macheroux P. (2016) Structure and biochemical properties of recombinant human dimethylglycine dehydrogenase and comparison to the disease-related H109R variant. *The FEBS Journal* **283**:3587-3603 https://doi.org/10.1111/febs.13828 | PubMed

[10] **Sánchez-Quitian Z. A.,** Schneider C. Z., Ducati R. G., de Azevedo W. F., Bloch C., Basso L. A., Santos D. S. (2010) Structural and functional analyses of Mycobacterium tuberculosis Rv3315c-encoded metal-dependent homotetrameric cytidine deaminase. *Journal of Structural Biology* **169**:413-423 https://doi.org/10.1016/j.jsb.2009.12.019 | PubMed

[11] **Teh A.-H.,** Kimura M., Yamamoto M., Tanaka N., Yamaguchi I., Kumasaka T. (2006) The 1.48 Å Resolution Crystal Structure of the Homotetrameric Cytidine Deaminase from Mouse. *Biochemistry* **45**:7825-7833 https://doi.org/10.1021/bi060345f | PubMed

[12] **Bergman T.,** Jörnvall H. (2013) Zinc Structural Site in Alcohol Dehydrogenases. In: Kretsinger R.H., Uversky V.N., Permyakov E.A. (Eds). *Encyclopedia of Metalloproteins* New York, NY: Springer. pp. 2518-2523

[13] **Jörnvall H.,** Bergman T. (2013) Zinc Alcohol Dehydrogenases. In: Kretsinger R.H., Uversky V.N., Permyakov E.A. (Eds). *Encyclopedia of Metalloproteins* New York, NY: Springer. pp. 2349-2354

[14] **Pihlaja K.,** Parkkinen A., Lönnberg H. (1983) Schiff's bases as intermediates in the hydrolytic decomposition of 2-alkyl-3-methyl-1,3-oxazolidines in aqueous acid. *J. Chem. Soc., Perkin Trans* **2**:1223-1226 https://doi.org/10.1039/p29830001223

[15] **Cappa F.,** Polidori N., Giuriato D., Correddu D., Marucco A., Sadeghi S. J., Levi R., Catucci G., Gilardi G. (2025) Calorimetric characterization of the stability and activity of trimethylamine-N-oxide (TMAO) demethylase from Methylocella silvestris BL2. *Protein Science* **34**:e70364 https://doi.org/10.1002/pro.70364 | PubMed

[16] **Lee H. H.,** Kim D. J., Ahn H. J., Ha J. Y., Suh S. W. (2004) Crystal Structure of T-protein of the Glycine Cleavage System: COFACTOR BINDING, INSIGHTS INTO H-PROTEIN RECOGNITION, AND MOLECULAR BASIS FOR UNDERSTANDING NONKETOTIC HYPERGLYCINEMIA *. *Journal of Biological Chemistry* **279**:50514-50523 https://doi.org/10.1074/jbc.m409672200 | PubMed

[17] **Kohls D.,** Sulea T., Purisima E. O., MacKenzie R. E., Vrielink A. (2000) The crystal structure of the formiminotransferase domain of formiminotransferase-cyclodeaminase: implications for substrate channeling in a bifunctional enzyme. *Structure* **8**:35-46 https://doi.org/10.1016/s0969-2126(00)00078-2 | PubMed

[18] **Luka Z.,** Pakhomova S., Loukachevitch L. V., Newcomer M. E., Wagner C. (2014) Folate in demethylation: The crystal structure of the rat dimethylglycine dehydrogenase complexed with tetrahydrofolate. *Biochemical and Biophysical Research Communications* **449**:392-398 https://doi.org/10.1016/j.bbrc.2014.05.064 | PubMed

[19] **Hyde C. C.,** Ahmed S. A., Padlan E. A., Miles E. W., Davies D. R. (1988) Three-dimensional structure of the tryptophan synthase alpha 2 beta 2 multienzyme complex from Salmonella typhimurium. *Journal of Biological Chemistry* **263**:17857-17871 https://doi.org/10.1016/s0021-9258(19)77913-7 | PubMed

[20] **Dunn M. F.** (2012) Allosteric regulation of substrate channeling and catalysis in the tryptophan synthase bienzyme complex. *Archives of Biochemistry and Biophysics* **519**:154-166 https://doi.org/10.1016/j.abb.2012.01.016 | PubMed

[21] **Douce R.,** Bourguignon J., Neuburger M., Rébeillé F. (2001) The glycine decarboxylase system: a fascinating complex. *Trends in Plant Science* **6**:167-176 https://doi.org/10.1016/s1360-1385(01)01892-1 | PubMed

[22] **Zhang H.,** Li Y., Nie J., Ren J., Zeng A.-P. (2020) Structure-based dynamic analysis of the glycine cleavage system suggests key residues for control of a key reaction step. *Commun Biol* **3**:756 https://doi.org/10.1038/s42003-020-01401-6 | PubMed

[23] **Sathyanarayanan N.,** Cannone G., Gakhar L., Katagihallimath N., Sowdhamini R., Ramaswamy S., Vinothkumar K. R. (2019) Molecular basis for metabolite channeling in a ring opening enzyme of the phenylacetate degradation pathway. *Nat Commun* **10**:4127 https://doi.org/10.1038/s41467-019-11931-1 | PubMed

[24] **Zhu Y.,** Jameson E., Parslow R. A., Lidbury I., Fu T., Dafforn T. R., Schäfer H., Chen Y. (2014) Identification and characterization of trimethylamine N-oxide (TMAO) demethylase and TMAO permease in Methylocella silvestris BL2. *Environmental Microbiology* **16**:3318-3330 https://doi.org/10.1111/1462-2920.12585 | PubMed

[25] **Zheng S. Q.,** Palovcak E., Armache J.-P., Verba K. A., Cheng Y., Agard D. A. (2017) MotionCor2: anisotropic correction of beam-induced motion for improved cryo-electron microscopy. *Nat Methods* **14**:331-332 https://doi.org/10.1038/nmeth.4193 | PubMed

[26] **Zhang K.** (2016) Gctf: Real-time CTF determination and correction. *Journal of Structural Biology* **193**:1-12 https://doi.org/10.1016/j.jsb.2015.11.003 | PubMed

[27] **Voss N. R.,** Yoshioka C. K., Radermacher M., Potter C. S., Carragher B. (2009) DoG Picker and TiltPicker: software tools to facilitate particle selection in single particle electron microscopy. *J Struct Biol* **166**:205-213 https://doi.org/10.1016/j.jsb.2009.01.004 | PubMed

[28] **Punjani A.,** Rubinstein J. L., Fleet D. J., Brubaker M. A. (2017) cryoSPARC: algorithms for rapid unsupervised cryo-EM structure determination. *Nat Methods* **14**:290-296 https://doi.org/10.1038/nmeth.4169 | PubMed

[29] **Emsley P.,** Cowtan K. (2004) Coot: model-building tools for molecular graphics. *Acta Cryst D* **60**:2126-2132 https://doi.org/10.1107/s0907444904019158 | PubMed

[30] **Jumper J.,** Evans R., Pritzel A., Green T., Figurnov M., Ronneberger O., Tunyasuvunakool K., Bates R., Žídek A., Potapenko A., *et al.* (2021) Highly accurate protein structure prediction with AlphaFold. *Nature* **596**:583-589 https://doi.org/10.1038/s41586-021-03819-2 | PubMed

[31] **Pettersen E. F.,** Goddard T. D., Huang C. C., Meng E. C., Couch G. S., Croll T. I., Morris J. H., Ferrin T. E. (2021) UCSF ChimeraX: Structure visualization for researchers, educators, and developers. *Protein Science* **30**:70-82 https://doi.org/10.1002/pro.3943 | PubMed

[32] **Afonine P. V.,** Poon B. K., Read R. J., Sobolev O. V., Terwilliger T. C., Urzhumtsev A., Adams P. D. (2018) Real-space refinement in PHENIX for cryo-EM and crystallography. *Acta Cryst D* **74**:531-544 https://doi.org/10.1107/s2059798318006551 | PubMed

[33] **Chen V. B.,** Wedell J. R., Wenger R. K., Ulrich E. L., Markley J. L. (2015) MolProbity for the masses–of data. *J Biomol NMR* **63**:77-83 https://doi.org/10.1007/s10858-015-9969-9 | PubMed

[34] **Pravda L.,** Sehnal D., Toušek D., Navrátilová V., Bazgier V., Berka K., Vařeková R. Svobodová, Koča J., Otyepka M. (2018) MOLEonline: a web-based tool for analyzing channels, tunnels and pores (2018 update). *Nucleic Acids Research* **46**:W368-W373 https://doi.org/10.1093/nar/gky309 | PubMed

[35] **DeLano W.L.** (2002) The PyMOL Molecular Graphics System. DeLano Scientific. http://www.pymol.org

[36] **Souza P. C. T.,** Borges-Araújo L., Brasnett C., Moreira R. A., Grünewald F., Park P., Wang L., Razmazma H., Borges-Araújo A. C., Cofas-Vargas L. F., *et al.* (2025) GōMartini 3: From large conformational changes in proteins to environmental bias corrections. *Nat Commun* **16**:4051 https://doi.org/10.1038/s41467-025-58719-0 | PubMed

[37] **Kroon P. C.,** Grunewald F., Barnoud J., van Tilburg M., Souza P. C. T., Wassenaar T. A., Marrink S. J. (2024) Martinize2 and Vermouth: Unified Framework for Topology Generation. *eLife* **12** https://doi.org/10.7554/eLife.90627.2

[38] **Joosten R. P.,** Beek T. A. H. te, Krieger E., Hekkelman M. L., Hooft R. W. W., Schneider R., Sander C., Vriend G. (2011) A series of PDB related databases for everyday needs. *Nucleic Acids Research* **39**:D411-D419 https://doi.org/10.1093/nar/gkq1105 | PubMed

[39] **Tironi I. G.,** Sperb R., Smith P. E., van Gunsteren W. F. (1995) A generalized reaction field method for molecular dynamics simulations. *The Journal of Chemical Physics* **102**:5451-5459 https://doi.org/10.1063/1.469273

[40] **Wassenaar T. A.,** Ingólfsson H. I., Böckmann R. A., Tieleman D. P., Marrink S. J. (2015) Computational Lipidomics with insane: A Versatile Tool for Generating Custom Membranes for Molecular Simulations. *J. Chem. Theory Comput* **11**:2144-2155 https://doi.org/10.1021/acs.jctc.5b00209 | PubMed

[41] **Bussi G.,** Donadio D., Parrinello M. (2007) Canonical sampling through velocity rescaling. *The Journal of Chemical Physics* **126**:014101 https://doi.org/10.1063/1.2408420 | PubMed

[42] **Parrinello M.,** Rahman A. (1981) Polymorphic transitions in single crystals: A new molecular dynamics method. *Journal of Applied Physics* **52**:7182-7190 https://doi.org/10.1063/1.328693

[43] **Chovancova E.,** Pavelka A., Benes P., Strnad O., Brezovsky J., Kozlikova B., Gora A., Sustr V. (2012) CAVER 3.0: A Tool for the Analysis of Transport Pathways in Dynamic Protein Structures. *PLOS Computational Biology* **8**:e1002708 https://doi.org/10.1371/journal.pcbi.1002708 | PubMed

# Peer reviews

## Reviewer #1 (Public review):

Summary:

Thach et al. report on the structure and function of trimethylamine N-oxide demethylase (TDM). They identify a novel complex assembly composed of multiple TDM monomers and obtain high-resolution structural information for the catalytic site, including an analysis of its metal composition, which leads them to propose a mechanism for the catalytic reaction.

In addition, the authors describe a novel substrate channel within the TDM complex that connects the N-terminal $ZnZn^{2+}$-dependent TMAO demethylation domain with the C-terminal tetrahydrofolate (THF)-binding domain. This continuous intramolecular tunnel appears highly optimized for shuttling formaldehyde (HCHO), based on its negative electrostatic properties and restricted width. The authors propose that this channel facilitates the safe transfer of HCHO, enabling its efficient conversion to methylenetetrahydrofolate (MTHF) at the C-terminal domain as a microbial detoxification strategy. Experimental data that shows an involvement of TDM in the reaction of HCHO with THF is less convincing.

Strengths:

The authors provide convincing high-resolution cryo-EM structural evidence (up to 2 Å) revealing an intriguing complex composed of two full monomers and two half-domains. They further present evidence for the metal ion bound at the active site and articulate a hypothesis for the catalytic cycle. Substantial effort is devoted to optimizing and characterizing enzyme activity, including detailed kinetic analyses across a range of pH values, temperatures, and substrate concentrations. Furthermore, the authors validate their structural insights through functional analysis of active-site point mutants.

In addition, the authors identify a continuous channel for formaldehyde (HCHO) passage within the structure and support this interpretation through molecular dynamics simulations. These analyses suggest an exciting mechanism of specific, dynamic, and gated channelling of HCHO. This finding is particularly appealing, as it implies the existence of a unique, completely enclosed conduit that may be of broad interest, including potential applications in bioengineering.

Weaknesses:

Although the idea of an enclosed channel for HCHO is compelling, the experimental evidence supporting enzymatic assistance in the reaction of HCHO with THF is less convincing. The linear regression analysis shown in Figure 1C demonstrates a THF concentration-dependent decrease in HCHO; however, it is well established that HCHO and THF can react spontaneously in a non-enzymatic manner, raising the possibility that the observed effect does not require enzymatic involvement. I appreciate the authors' clarification that the data in Figure 1 were not intended to demonstrate enzymatic channelling or catalytic involvement in the HCHO-THF reaction, and that the assay does not distinguish between changes in HCHO production and downstream consumption. However, the statement "these findings show that TDM carries out two linked reactions: TMAO demethylation at one active site, and the HCHO produced can condense with THF at the C-terminal domain, connecting TMAO breakdown to one-carbon metabolism" (page 2) still implies a mechanistic and functional coupling that is not supported by the presented data and appears inconsistent with the authors' clarification. In light of this, I recommend revising this statement to avoid implying mechanistic or functional coupling between the two reactions unless additional experimental evidence is provided.

Overall, the authors were successful in advancing our structural and functional understanding of the TDM complex. They suggest an interesting oligomeric complex composition which should be investigated with additional biophysical techniques.

Additionally, they provide an intriguing hypothesis for a new type of substrate channelling. Additional kinetic experiments focusing on HCHO and THF turnover by enzymatic proximity effects would strengthen this potentially fundamental finding. If this channelling mechanism can be supported by stronger experimental evidence, it would substantially advance our understanding and knowledge of biologic conduits and enable future efforts in the design of artificial cascade catalysis systems with high conversion rate and efficiency, as well as detoxification pathways.

https://doi.org/10.7554/eLife.109964.2.sa2

## Reviewer #2 (Public review):

Summary:

The manuscript reports a cryo-EM structure of TMAO demethylase from Paracoccus sp. This is an important enzyme in the metabolism of trimethylamine oxide (TMAO) and trimethylamine (TMA) in human gut microbiota, so new information about this enzyme would certainly be of interest.

Strengths:

The cryo-EM structure for this enzyme is new and provides new insights into the function of the different protein domains, and a channel for formaldehyde between the two domains.

Weaknesses:

(1) The proposed catalytic mechanism in this manuscript does not make sense. Previous mechanistic studies on the Methylocella silvestris TMAO demethylase (FEBS Journal 2016, 283, 3979-3993, reference 7) reported that, as well as a Zn2+ cofactor, there was a dependence upon non-heme Fe2+, and proposed a catalytic mechanism involving deoxygenation to form TMA and an iron(IV)-oxo species, followed by oxidative demethylation to form DMA and formaldehyde.

In this work, the authors do not mention the previously proposed mechanism, but instead just say that elemental analysis "excluded iron". This is alarming, since the previous work has a key role for non-heme iron in the mechanism. The elemental analysis here gives a Zn content of about 0.5 mol/mol protein (and no Fe), whereas the Methylocella TMAO demethylase was reported to contain 0.97 mol Zn/mol protein, and 0.35-0.38 mol Fe/mol protein. It does, therefore, appear that their enzyme is depleted in Zn, and the absence of Fe impacts on the mechanism, as explained below.

The proposed catalytic mechanism in this manuscript, I am sorry to say, does not make sense, for several reasons:

i) Demethylation to form formaldehyde is not a hydrolytic process; it is an oxidative process (normally accomplished by either cytochrome P450 or non-heme iron-dependent oxygenase). The authors propose that a zinc (II) hydroxide attacks the methyl group, which (a) is unprecedented, (b) even if it were possible, would generate methanol, not formaldehyde.

ii) The amine oxide is proposed to deoxygenate, with hydroxide appearing on the Zn - unfortunately, amine oxide deoxygenation is a reductive process, for which a reducing agent is needed, and $Zn^{2+}$ is not a redox active metal ion;

iii) The authors say "forming a tetrahedral intermediate, as described for metalloprotease" but zinc metalloproteases attack an amide carbonyl to form an oxyanion intermediate, whereas in this mechanism there is no carbonyl to attack, so this statement is just wrong.

So on several counts the proposed mechanism cannot be correct. Some redox cofactor is needed in order to carry out amine oxide deoxygenation, and $Zn^{2+}$ cannot fulfil that role. $Fe^{2+}$ could do, which is why the previously proposed mechanism involving an iron(IV)-oxo intermediate is feasible. But the authors claim that their enzyme has no Fe. If so then there must be some other redox cofactor present. Therefore, the authors need to re-analyse their enzyme carefully and look either for Fe or for some other redox-active metal ion, and then provide convincing experimental evidence for a feasible catalytic mechanism. As it stands the proposed catalytic mechanism is unacceptable.

Revised version. The authors have essentially not changed the proposed mechanism. They have removed the reference to zinc metalloproteases, but still propose a mechanism mediated only by $Zn^{2+}$. As explained above, attack by zinc (II) hydroxide is unprecedented and would generate methanol, not formaldehyde, and amine deoxygenation is a reductive process that cannot be fulfilled by $Zn^{2+}$. So the proposed mechanism is still not feasible at all. The authors now say that "oxidative chemistry....remains unresolved", I'm sorry, but that is not acceptable.

I have urged the authors to re-examine the metal content of their enzyme, In the Supporting Information (Figure S5) they give ICPMS data that indicates a Zn stoichiometry of 0.5 mol Zn/mol protein, and Fe is not detected. Have the authors analysed for other redox active metals? The authors say that there is no evidence for any other metal binding site, but there is only 50% occupancy of Zn in their protein, so could there be a different metal ion present in place of Zn in the other 50% of the protein, that accounts for the observed activity?

Since there is clearly a major discrepancy here, the onus is on the authors to explain the discrepancy, rather than just returning with the same data. For example, they could treat the enzyme with EDTA to remove all metals (and check the treated enzyme by ICPMS), and then add different metal ions to test activity with different metals (could even titrate with different molar equivalents of metal ions). They could then test a range of different redox-active metal ions.

(2) Given the metal content reported here, it is important to be able to compare the specific activity of the enzyme reported here with earlier preparations. The authors have now done

this in the revised version.

(3) The consumption of formaldehyde to form methylene-THF is potentially interesting, but the authors say "HCHO levels decreased in the presence of THF", which could potentially be due to enzyme inhibition by THF. Is there evidence that this is a time-dependent and protein-dependent reaction? Not yet addressed.

Also in Figure 1C, HCHO reduction (%) is not very helpful, because we don't know what concentration of formaldehyde is formed under these conditions; it would be better to quote in units of concentration, rather than %. This point has been addressed by the authors in the revised version.

(4) Has this particular TMAO demethylase been reported before? It's not clear which Paracoccus strain the enzyme is from; the Experimental Section just says "Paracoccus sp.", which is not very precise. There has been published work on the Paracoccus PS1 enzyme, is that the strain used? Details about the strain are needed, and the accession for the protein sequence. Addressed in the revised version.

https://doi.org/10.7554/eLife.109964.2.sa1

## Author response:

The following is the authors' response to the original reviews.

> ***Public Reviews:***
>
> ***Reviewer #1 (Public review):***
>
> *Summary:*
>
> *Thach et al. report on the structure and function of trimethylamine N-oxide demethylase (TDM). They identify a novel complex assembly composed of multiple TDM monomers and obtain high-resolution structural information for the catalytic site, including an analysis of its metal composition, which leads them to propose a mechanism for the catalytic reaction.*
>
> *In addition, the authors describe a novel substrate channel within the TDM complex that connects the N-terminal $Zn^2$-dependent TMAO demethylation domain with the C-terminal tetrahydrofolate (THF)-binding domain. This continuous intramolecular tunnel appears highly optimized for shuttling formaldehyde (HCHO), based on its negative electrostatic properties and restricted width. The authors propose that this channel facilitates the safe transfer of HCHO, enabling its efficient conversion to methylenetetrahydrofolate (MTHF) at the C-terminal domain as a microbial detoxification strategy.*
>
> *Strengths:*
>
> *The authors provide convincing high-resolution cryo-EM structural evidence (up to 2 Å) revealing an intriguing complex composed of two full monomers and two half-domains. They further present evidence for the metal ion bound at the active site and articulate a plausible hypothesis for the catalytic cycle. Substantial effort is devoted to optimizing and characterizing enzyme activity, including detailed kinetic analyses across a range of pH values, temperatures, and substrate concentrations. Furthermore, the authors validate their structural insights through functional analysis of active-site point mutants.*
>
> *In addition, the authors identify a continuous channel for formaldehyde (HCHO) passage within the structure and support this interpretation through molecular dynamics simulations. These analyses suggest an exciting mechanism of specific, dynamic, and gated channeling of HCHO. This finding is particularly appealing, as it implies the*

> *existence of a unique, completely enclosed conduit that may be of broad interest, including potential applications in bioengineering.*
>
> *Weaknesses:*
>
> *Although the idea of an enclosed channel for HCHO is compelling, the experimental evidence supporting enzymatic assistance in the reaction of HCHO with THF is less convincing. The linear regression analysis shown in Figure 1C demonstrates a THF concentration-dependent decrease in HCHO, but the concentrations used for THF greatly exceed its reported KD (enzyme concentration used in this assay is not reported). It has previously been shown that HCHO and THF can couple spontaneously in a non-enzymatic manner, raising the possibility that the observed effect does not require enzymatic channeling. An additional control that can rule out this possibility would help to strengthen the evidence. For example, mutating the THF binding site to prevent THF binding to the protein complex could clarify whether the observed decrease in HCHO depends on enzyme-mediated proximity effects. A mutation which would specifically disable channeling could be even more convincing (maybe at the narrowest bottleneck).*

We agree with the reviewer that HCHO and THF can react spontaneously in a non-enzymatic manner, and our experiments were not intended to demonstrate enzymatic channeling. The linear regression analysis in Figure 1C was designed solely to confirm that HCHO reacts with THF under our assay conditions. Accordingly, THF was titrated over a broad concentration range starting from zero, and the observed THF concentration–dependent decrease in HCHO reflects this chemical reactivity.

We do not interpret these data as evidence that the enzyme catalyzes or is required for the HCHO–THF coupling reaction. Instead, the structural observation of an enclosed channel is presented as a separate finding. We have clarified this point in the revised text to avoid overinterpretation of the biochemical data (page 2, line 16).

> *Another concern is that the observed decrease in HCHO could alternatively arise from a reduced production of HCHO due to a negative allosteric effect of THF binding on the active site. From this perspective, the interpretation would be more convincing if a clear coupled effect could be demonstrated, specifically, that removal of the product (HCHO) from the reaction equilibrium leads to an increase in the catalytic efficiency of the demethylation reaction.*

We agree that, in principle, a decrease in detectable HCHO could also arise from an indirect effect of THF binding on enzyme activity. However, in our study the experiment was not designed to assess catalytic coupling or allosteric regulation. The assay in question monitors HCHO levels under defined conditions and does not distinguish between changes in HCHO production and downstream consumption.

Additionally, we do not interpret the observed decrease in HCHO as evidence that THF binding enhances catalytic efficiency, or that removal of HCHO shifts the reaction equilibrium. Instead, the data are presented to establish that HCHO can react with THF under the assay conditions. Any potential allosteric effects of THF on the demethylation reaction, or kinetic coupling between HCHO removal and catalysis, are beyond the scope of the current study, and are not claimed.

> *While the enzyme kinetics appear to have been performed thoroughly, the description of the kinetic assays in the Methods section is very brief. Important details such as reaction buffer composition, cofactor identity and concentration ($Zn^{2+}$), enzyme concentration, defined temperature, and precise pH are not clearly stated. Moreover, a detailed methodological description could not be found in the cited reference (6), if I am not mistaken.*

Thank you for the suggestion. We have added reference [24] to the methodological description on page 8. The Methods section has been revised accordingly on page 8 under "TDM Activity Assay," without altering the $Zn^{2+}$ concentration.

> *The composition of the complex is intriguing but raises some questions. Based on SDS-PAGE analysis, the purified protein appears to be predominantly full-length TDM, and size-exclusion chromatography suggests an apparent molecular weight below 100 kDa. However, the cryo-EM structure reveals a substantially larger complex composed of two full-length monomers and two half-domains.*

We appreciate the reviewer's careful analysis of the apparent discrepancy between the biochemical characterization and the cryo-EM structure. This issue is addressed in Figure S1, which may have been overlooked.

As shown in Figure S1, the stability of TDM is highly dependent on protein and salt conditions. At 150 mM NaCl, SEC reveals a dominant peak eluting between 10.5 and 12 mL, corresponding to an estimated molecular weight of ~170–305 kDa (blue dot, Author response image 1). This fraction was explicitly selected for cryo-EM analysis and yields the larger complex observed in the reconstruction. At lower salt concentrations (50 mM) or higher (>150 mM NaCl), the protein either aggregates or elutes near the void volume (~8 mL).

SDS–PAGE analysis detects full-length TDM together with smaller fragments (~40–50 kDa and ~22–25 kDa). The apparent predominance of full-length protein on SDS–PAGE likely reflects its greater staining intensity per molecule and/or a higher population, rather than the absence of truncated species.

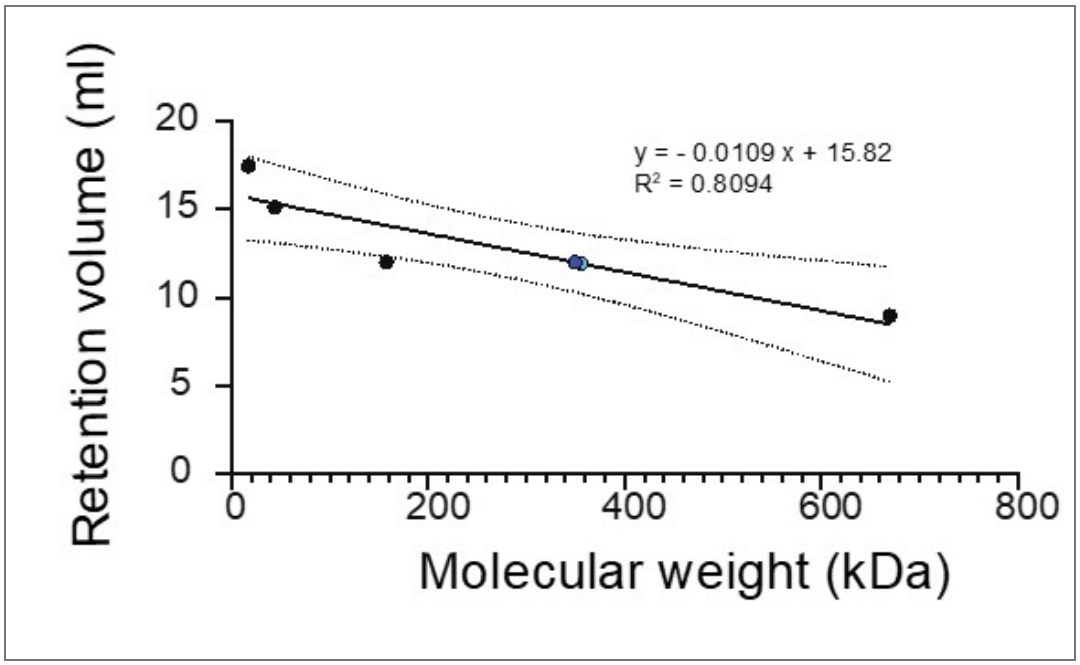


**Author response image 1.**

> *Given the lack of clear evidence for proteolytic fragments on the SDS-PAGE gel, it is unclear how the observed stoichiometry arises. This raises the possibility of higher-order assemblies or alternative oligomeric states. Did the authors attempt to pick or analyze larger particles during cryo-EM processing? Additional biophysical characterization of particle size distribution - for example, using interferometric scattering microscopy (iSCAT)-could help clarify the oligomeric state of the complex in solution.*

Cryo-EM data were collected exclusively from the size-exclusion chromatography fraction eluting between 10.5 and 12 mL. This fraction was selected to isolate the dominant assembly in solution. Extensive 2D and 3D particle classification did not reveal distinct classes corresponding to smaller species or higher-order oligomeric assemblies. Instead, the vast majority of particles converged to a single, well-defined structure consistent with the 2 full-length + 2 half-domain stoichiometry.

A minor subpopulation (~2%) exhibited increased flexibility in the N-terminal region of the two full-length subunits, but these particles did not form a separate oligomeric class, indicating conformational heterogeneity rather than alternative assembly states (Author response image 2). Together, these data support the 2+2½ architecture as the predominant and stable complex under the conditions used for cryo-EM. Additional techniques, such as iSCAT, would provide complementary information, but are not required to support the conclusions drawn from the SEC and cryo-EM analyses presented here.

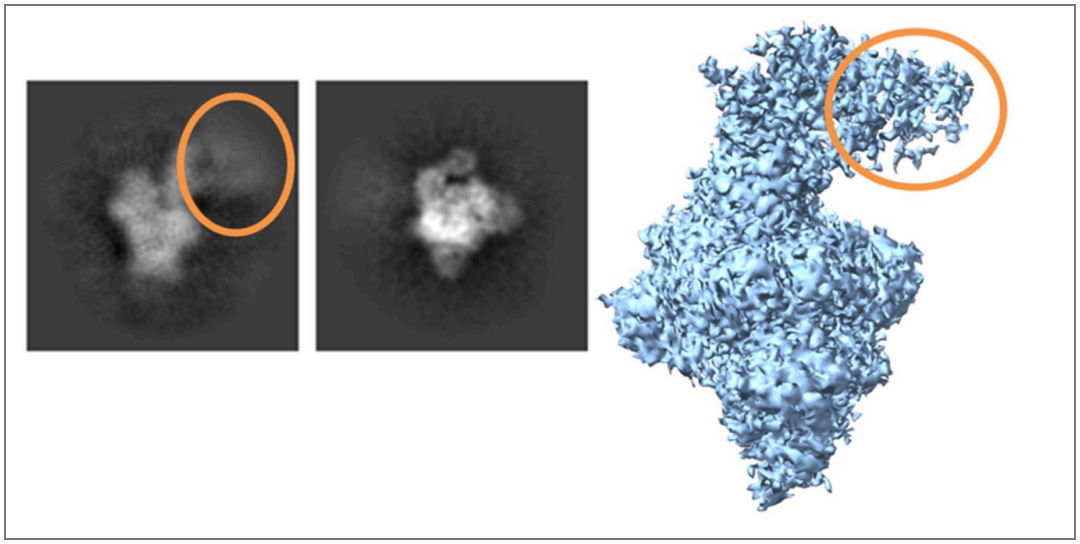

**Author response image 2.**

> *The authors mention strict symmetry in the complex, yet C2 symmetry was enforced during refinement. While this is reasonable as an initial approach, it would strengthen the structural interpretation to relax the symmetry to C1 using the C2-refined map as a reference. This could reveal subtle asymmetries or domain-specific differences without sacrificing the overall quality of the reconstruction.*

We thank the reviewer for this thoughtful suggestion. In standard cryo-EM data processing, symmetry is typically not imposed initially to minimize potential model bias; accordingly, we first performed C1 refinement before applying C2 symmetry. The resulting C1 reconstructions revealed no detectable asymmetry or domain-specific differences relative to the C2 map. In addition, relaxing the symmetry consistently reduced overall resolution, indicating lower alignment accuracy and further supporting the presence of a predominantly symmetric assembly.

> *In this context, the proposed catalytic role of $Zn^{2+}$ raises additional questions. Why is a 2:1 enzyme-to-metal stoichiometry observed, and how does this reconcile with previous reports? This point warrants discussion. Does this imply asymmetric catalysis within the complex? Would the stoichiometry change under $Zn^{2+}$-saturating conditions, as no $Zn^{2+}$ appears to be added to the buffers? It would be helpful to clarify whether $Zn^{2+}$ occupancy is equivalent in both active sites when symmetry is not imposed, or whether partial occupancy is observed.*

The observed ~2:1 enzyme-to-$Zn^{2+}$ stoichiometry likely reflects the composition of the 2 full-length + 2 half-domain (2+2½) complex. In this assembly, only the core domains that are fully present in the complex contribute to metal binding. The truncated or half-domains lack the $Zn^{2+}$ binding domain. As a result, only two metal-binding sites are occupied per assembled complex, consistent with the measured stoichiometry.

We note that $Zn^{2+}$ was not deliberately added to the buffers, so occupancy may not reflect full saturation. Based on our cryo-EM and biochemical data, both metal-binding sites in the full-length subunits appear to be occupied to an equivalent extent, and no clear evidence of asymmetric catalysis is observed under these current experimental conditions. Full $Zn^{2+}$ saturation could potentially increase occupancy, but was not explored in these experiments.

> *The divalent ion $Zn^{2+}$ is suggested to activate water for the catalytic reaction. I am not sure if there is a need for a water molecule to explain this catalytic mechanism. Can you please elaborate on this more? As one aspect, it might be helpful to explain in more detail how Zn-OH and D220 are recovered in the last step before a new water molecule comes in.*

Thank you for your suggestion. We revised our text in page 2 as bellow.

Based on our structural and biochemical data, we propose a structurally informed working model for TMAO turnover by TDM (Scheme 1). In this model, $Zn^{2+}$ plays a non-redox role by polarizing the O–H bond of the bound hydroxyl, thereby lowering its $pK_a$. The D220 carboxylate functions as a general base, abstracting the proton to generate a hydroxide nucleophile. This hydroxide then attacks the electrophilic N-methyl carbon of TMAO, forming a tetrahedral carbinolamine (hemiaminal) intermediate. Subsequent heterolytic cleavage of the C–N bond leads to the release of HCHO. D220 then switches roles to act as a general acid, donating a proton to the departing nitrogen, which facilitates product release and regenerates the active site. This sequence allows a new water molecule to rebind $Zn^{2+}$, enabling subsequent catalytic turnovers. This proposed pathway is consistent with prior mechanistic studies, in which water addition to the azomethine carbon of a cationic Schiff base generates a carbinolamine intermediate, followed by a rate-limiting breakdown to yield an amino alcohol and a carbonyl compound, in the published case, an aldehyde (Pihlaja et al., J. Chem. Soc. Perkin Trans. 2, 1983, 8, 1223–1226).

> *Overall, the authors were successful in advancing our structural and functional understanding of the TDM complex. They suggest an interesting oligomeric complex composition which should be investigated with additional biophysical techniques.*
>
> *Additionally, they provide an intriguing hypothesis for a new type of substrate channeling. Additional kinetic experiments focusing on HCHO and THF turnover by enzymatic proximity effects would strengthen this potentially fundamental finding. If this channeling mechanism can be supported by stronger experimental evidence, it would substantially advance our understanding and knowledge of biologic conduits and enable future efforts in the design of artificial cascade catalysis systems with high conversion rate and efficiency, as well as detoxification pathways.*
>
> ***Reviewer #2 (Public review):***

*Summary:*

*The manuscript reports a cryo-EM structure of TMAO demethylase from Paracoccus sp. This is an important enzyme in the metabolism of trimethylamine oxide (TMAO) and trimethylamine (TMA) in human gut microbiota, so new information about this enzyme would certainly be of interest.*

*Strengths:*

*The cryo-EM structure for this enzyme is new and provides new insights into the function of the different protein domains, and a channel for formaldehyde between the two domains.*

*Weaknesses:*

*(1) The proposed catalytic mechanism in this manuscript does not make sense. Previous mechanistic studies on the Methylocella silvestris TMAO demethylase (FEBS Journal 2016, 283, 3979-3993, reference 7) reported that, as well as a Zn2+ cofactor, there was a dependence upon non-heme Fe2+, and proposed a catalytic mechanism involving deoxygenation to form TMA and an iron(IV)-oxo species, followed by oxidative demethylation to form DMA and formaldehyde.*

*In this work, the authors do not mention the previously proposed mechanism, but instead say that elemental analysis "excluded iron". This is alarming, since the previous work has a key role for non-heme iron in the mechanism. The elemental analysis here gives a Zn content of about 0.5 mol/mol protein (and no Fe), whereas the Methylocella TMAO demethylase was reported to contain 0.97 mol Zn/mol protein, and 0.35-0.38 mol Fe/mol protein. It does, therefore, appear that their enzyme is depleted in Zn, and the absence of Fe impacts the mechanism, as explained below.*

*The proposed catalytic mechanism in this manuscript, I am sorry to say, does not make sense to me, for several reasons:*

*(i) Demethylation to form formaldehyde is not a hydrolytic process; it is an oxidative process (normally accomplished by either cytochrome P450 or non-heme iron-dependent oxygenase). The authors propose that a zinc (II) hydroxide attacks the methyl group, which is unprecedented, and even if it were possible, would generate methanol, not formaldehyde.*

*(ii) The amine oxide is then proposed to deoxygenate, with hydroxide appearing on the Zn - unfortunately, amine oxide deoxygenation is a reductive process, for which a reducing agent is needed, and Zn2+ is not a redox-active metal ion;*

*(iii) The authors say "forming a tetrahedral intermediate, as described for metalloproteinase", but zinc metalloproteases attack an amide carbonyl to form an oxyanion intermediate, whereas in this mechanism, there is no carbonyl to attack, so this statement is just wrong.*

*So on several counts, the proposed mechanism cannot be correct. Some redox cofactor is needed in order to carry out amine oxide deoxygenation, and Zn2+ cannot fulfil that role. Fe2+ could do, which is why the previously proposed mechanism involving an iron(IV)-oxo intermediate is feasible. But the authors claim that their enzyme has no Fe. If so, then there must be some other redox cofactor present. Therefore, the authors need to re-analyse their enzyme carefully and look either for Fe or for some other redox-active metal ion, and then provide convincing experimental evidence for a feasible catalytic mechanism. As it stands, the proposed catalytic mechanism is unacceptable.*

We thank the reviewer for the detailed and thoughtful mechanistic critique. We fully agree that $Zn^{2+}$ is not redox-active, and cannot directly mediate oxidative demethylation or amine oxide deoxygenation. We acknowledge that the oxidative step required for the conversion of TMAO to HCHO is not explicitly resolved in the present study. Accordingly, we have revised the manuscript to remove any implication of $Zn^{2+}$-mediated redox chemistry, and have eliminated the previously imprecise analogy to zinc metalloproteases.

We recognize and now discuss prior biochemical work on TMAO demethylase from *Methylocella silvestris* (MsTDM), which proposed an iron-dependent oxidative mechanism (Zhu et al., FEBS 2016, 3979–3993). That study reported approximately one $Zn^{2+}$ and one non-heme $Fe^{2+}$ per active enzyme, implicated iron in catalysis through homology modeling and mutagenesis, and used crossover experiments suggesting a trimethylamine-like intermediate and oxygen transfer from TMAO, consistent with an Fe-dependent redox process. However, that system lacked experimental structural information, and did not define discrete metal-binding sites.

In contrast,

(1) Our high-resolution cryo-EM structures and metal analyses of TDM consistently reveal only a single, well-defined $Zn^{2+}$-binding site, with no structural evidence for an additional iron-binding site as in the previous report (Zhu et al., FEBS 2016, 3979–3993).

(2) To investigate the potential involvement of iron, we expressed TDM in LB medium supplemented with $Fe(NH_4)_2SO_4$ and determined its cryo-EM structure. This structure is identical to the original one, and no EM density corresponding to a second iron ion was observed. Moreover, the previously proposed $Fe^{2+}$-binding residues are spatially distant (Figure S6).

(3) ICP-MS analysis shows undetectable Iron, and only Zinc ion (Figure S5).

(4) Our enzyme kinetics analysis with the TDM without Iron is comparable to that of from MsTDM (Figure 1A). The differences in Km and Vmax we propose is due to the difference in the overall sequence of the enzymes. Please also see comment at the end on a new published paper on MsTDM.

While we cannot comment on the MsTDM results, our ‘experimental’ results do not support the presence of an iron-binding site. Our data indicate that this chemistry is unlikely to be mediated by a canonical non-heme iron center as proposed for MsTDM. We therefore revised our model as a structural framework that rationalizes substrate binding, metal coordination, and product stabilization, while clearly delineating the limits of mechanistic inference supported by the current data.

The scheme 1 and proposal mechanism section were revised in page 4. Figure S6 was added.

> *(2) Given the metal content reported here, it is important to be able to compare the specific activity of the enzyme reported here with earlier preparations. The authors do quote a Vmax of 16.52 μM/min/mg; however, these are incorrect units for Vmax, they should be μmol/min/mg. There is a further inconsistency between the text saying μM/min/mg and the Figure saying μM/min/μg.*

Thank you for the correction. We converted the $V_{max}$ unit to nmol/min/mg. and revised the text in page 2. We also compared with the value of the previous report in the TDM enzyme by revising the text on page 2. See also the note on a newly published manuscript and its comparison.

> *(3) The consumption of formaldehyde to form methylene-THF is potentially interesting, but the authors say "HCHO levels decreased in the presence of THF", which could potentially be due to enzyme inhibition by THF. Is there evidence that this is a time-dependent and protein-dependent reaction? Also in Figure 1C, HCHO reduction (%) is not very helpful, because we don't know what concentration of formaldehyde is formed*

> *under these conditions; it would be better to quote in units of concentration, rather than %.*

We appreciate this important point. We have revised Figure 1C to present HCHO levels in absolute concentration units. While the current data demonstrate reduced detectable HCHO in the presence of THF, we agree that distinguishing between HCHO consumption and potential THF-mediated enzyme inhibition would require dedicated time-course and protein-dependence experiments. We have therefore revised the description to avoid overinterpretation and limit our conclusions to the observed changes in HCHO concentration in page 2, line 18-19.

> *(4) Has this particular TMAO demethylase been reported before? It's not clear which Paracoccus strain the enzyme is from; the Experimental Section just says "Paracoccus sp.", which is not very precise. There has been published work on the Paracoccus PS1 enzyme; is that the strain used? Details about the strain are needed, and the accession for the protein sequence.*

Thank you for this comment. We now indicate that the enzyme is derived from *Paracoccus* sp. DMF and provide the accession number for the protein sequence (WP_263566861) in the Experimental Section (page 8, line 4).

> ***Recommendations for the authors:***
>
> ***Reviewer #1 (Recommendations for the authors):***
>
> *(1) The ITC experiment requires a ligand-into-buffer titration as an additional control. Also, maybe I misunderstood the molar ratio or the concentrations you used, but if you indeed added a total of 4.75 µL of 20 µM THF into 250 µL of 5 µM TDM, it is not clear to me how this leads to a final molar ratio of 3.*

We thank the reviewer for this suggestion. A ligand-into-buffer control ITC experiment was performed and is now included in Figure S8C, which shows no realizable signal.

Regarding the molar ratio, it is our mistake. The experiment used 2.45 µL injections of 80 µM THF into 250 µL of 5 µM TDM. This corresponds to a final ligand concentration of ~12.8 µM, giving a ligand-to-protein molar ratio of ~2.6. We revised our text in page 9, ITC section.

> *(2) Characterization/quality check of all mutant enzymes should be performed by NanoDSF, CD spectroscopy or similar techniques to confirm that proteins are properly folded and fit for kinetic testing.*

We appreciate the reviewer's suggestion. All mutant proteins, including D220A, D367A, and F327A, were purified with yields similar to the wild-type enzyme. Additionally, cryo-EM maps of the mutants show well-defined density and overall structural integrity consistent with the wild-type. These findings indicate that the introduced mutations do not significantly affect protein folding, supporting their use for kinetic analysis. While NanoDSF might reveal differences in thermal stability due to mutations, it does not provide structural information. Our conclusions are not based on minor differences in thermostability. Our cryo-EM structures of the mutants offer much more reliable structural data than CD spectroscopy.

> *(3) Best practice would suggest overlapping pH ranges between different buffer systems in the pH-dependence experiments to rule out buffer-specific effects independent of pH.*

We thank the reviewer for this helpful suggestion. We agree that overlapping pH ranges between different buffer systems can be valuable for excluding buffer-specific effects. In this study, the pH-dependence experiments were intended to provide a qualitative assessment of pH sensitivity rather than a detailed analysis of buffer-independent pKa values. While we cannot fully exclude minor buffer-specific contributions, the overall trends observed were reproducible and sufficient to support the conclusions drawn. We have added a clarifying statement to the revised manuscript to reflect this consideration, page 2, line 12.

> *(4) Structural comparison revealed high similarity to a THF-binding protein, with superposition onto a T protein.": It would be nice to show this as an additional figure, as resolution and occupancy for THF are low.*

We thank the reviewer for this suggestion. To address this point, we have revised Figure S6 by adding an additional panel (C, now is Figure S7C) showing the structural superposition of TDM with the THF-binding T protein. This comparison is included to better illustrate the structural similarity, despite the limited resolution and partial occupancy of THF density in our map.

> *(5) Editing could have been done more thoroughly. Some spelling mistakes, e.g. "RESEULTS", "redius", "complec"; kinetic rate constants should be written in italic (not uniform between text and figures); Prism version is missing; Vmax of 16.52 µM/min/mg - doublecheck units; Figure S1B: The "arrow on the right" might have gone missing.*

We corrected the spelling in page 2 ~ line 10, page 5 ~ line 34, page 6 ~ line40. All were highlighted as blue color. Prism version was added. The arrow was added into figure S1B. The Vmax unit is corrected to nmol/min/mg

> ***Reviewer #2 (Recommendations for the authors):***
>
> *(1) The authors must re-examine the metal content of their purified enzyme, looking in particular for Fe or another redox-active metal ion, which could be involved in a reasonable catalytic mechanism.*

We thank the reviewer for this suggestion and have carefully re-examined the metal content of TDM. Elemental analyses by EDX and ICP-MS consistently detected $Zn^{2+}$ in purified TDM (Zn:protein ≈ 1:2), whereas Fe was below the detection limit across multiple independent preparations (Fig. S5A,B). To assess whether iron could be incorporated or play a functional role, we expressed TDM in *E. coli* grown in LB medium supplemented with $Fe(NH_4SO_4)_2$ and performed activity assays in the presence of exogenous $Fe^{2+}$. Neither condition resulted in enhanced enzymatic activity.

Consistent with these biochemical data, all cryo-EM structures reveal a single, well-defined metal-binding site coordinated by three conserved cysteine residues and occupied by $Zn^{2+}$, with no evidence for an additional iron species or other redox-active metal site.

> *(2) The specific activity of the enzyme should be quoted in the same units as other literature papers, so that the enzyme activity can be compared. It could be, for example, that the content of Fe (or other redox-active metal) is low, and that could then give rise to a low specific activity.*

Thank you for the suggestion, we quoted the enzyme units as similar with previous report. and revised the text in in page 2.

Since the submission of our paper a new report on MsTDM has been published (Cappa et al., Protein Science 33(11), e70364). It further supports our findings. First, the reported kinetic parameters using ITC (Vmax = 0.309 µmol/s, approximately 240 nmol/min/mg; Km = 0.866 mM) are comparable to our observed (156 nmol/min/mg and 1.33 mM, respectively) in the absence of exogenous iron. Second, the optimal pH for enzymatic activity similar to that observed in our paraTDM. Third, the reported two-state unfolding behavior is consistent with our cryo-EM structural observations, in which the more dynamic subunits appear to destabilize prior to unfolding of the core domains. Based on these findings, we now propose that $Zn^{2+}$ appears to function primarily as an organizational cofactor at the core catalytic domain (revised Scheme 1).

https://doi.org/10.7554/eLife.109964.2.sa0